

# **The Kiloparsec-Scale Structure and Kinematics of High-Redshift Star-Forming Galaxies**

**David R. Law**

**DISSERTATION.COM**



Boca Raton

*The Kiloparsec-Scale Structure and Kinematics of High-Redshift Star-Forming Galaxies*

Copyright © 2008 David R. Law

All rights reserved. No part of this book may be reproduced or transmitted in any form or by any means, electronic or mechanical, including photocopying, recording, or by any information storage and retrieval system, without written permission from the publisher.

Dissertation.com  
Boca Raton, Florida  
USA • 2008

ISBN-10: 1-59942-691-9  
ISBN-13: 978-1-59942-691-4

## Acknowledgements

The thesis has been made possible by the aid of a large number of people who are deserving of my profound thanks. Dawn Erb, Naveen Reddy, Kurt Adelberger, and Alice Shapley always had a kind and helpful word for me as a beginning graduate student, and taught me many of the practical skills necessary to accomplish this work. I have been privileged to follow in their footsteps. Thank you also to Max Pettini for his eternally cheery correspondence, Milan Bogosavljević for countless 4AM discussions on the meaning of life, the universe, and everything while staring at fuzzy stars from Palomar, and James Larkin, Shelley Wright, and the rest of the OSIRIS team whose hard work made possible the observational backbone of this thesis. To Karín Menéndez-Delmestre and Thiago Gonçalves, whose friendship and help during the last 5 years has been a blessing. Kathy DeGioia-Eastwood, Kathryn Johnston, and Steve Majewski encouraged and supported me during my first forays into the world of research astronomy and are in large part responsible for convincing me to pursue graduate study, as is Mark Freeman who made me think that the physics of orbiting bodies was interesting in the first place. Thank you particularly to Chuck Steidel for advising and supporting me during the last 5 years. I appreciate equally his patience, scientifically sceptical nature, and uncannily accurate insights. To my parents, Clare and Richard Law, who taught me the value of rational inquiry (whether it be the nature of the heavens or of the Earth) and without whose unconditional support and encouragement none of this would have been possible. Finally, thank you to my wife, Sarah, for her patience, understanding, and indomitable spirit which provides an unfailing source of inspiration.

# The Kiloparsec-Scale Structure and Kinematics of High-Redshift Star-Forming Galaxies

by

David R. Law

In Partial Fulfillment of the  
Requirements for the Degree of  
Doctor of Philosophy

## Abstract

We study the spatially resolved properties of star-forming galaxies at redshift  $z \sim 2 - 3$  on scales  $\sim 1$  kpc using a combination of morphological and kinematic analyses in an effort to characterize the major mechanisms of galaxy formation in the young universe. Using a sample of 216 galaxies which have been spectroscopically confirmed to lie between redshifts  $z = 1.8 - 3.4$  in the GOODS-N field we demonstrate that rest-UV morphology (as seen by the *Hubble Space Telescope*) is statistically uncorrelated with physical properties such as star formation rate and is therefore unable to support the hypothesis that the prevalence of irregular morphologies indicates a high major merger fraction. Further, we present a sample of 13 galaxies observed with the OSIRIS integral field spectrograph and the Keck laser-guide star adaptive optics system which demonstrate the prevalence of high velocity dispersions  $\sim 80 \text{ km s}^{-1}$  and generally little in the way of spatially resolved velocity gradients, inconsistent with favored rotating disk models. We discuss the implications of these results for galaxy formation models, including gas accretion via cold flows and gravitational instability of early gas-rich galactic disks. There is some evidence for a trend towards stronger rotational signatures in galaxies with more massive stellar populations.

# Contents

<b>List of Figures</b>	<b>x</b>
<b>List of Tables</b>	<b>xiii</b>
<b>1 Introduction</b>	<b>1</b>
1.1 MORPHOLOGY . . . . .	3
1.2 KINEMATICS . . . . .	4
<b>2 The Physical Nature of Rest-UV Galaxy Morphology During the Peak Epoch of Galaxy Formation</b>	<b>6</b>
2.1 INTRODUCTION . . . . .	7
2.2 SAMPLE SELECTION . . . . .	9
2.3 MORPHOLOGIES . . . . .	10
2.3.1 Pixel Selection . . . . .	17
2.3.2 The Size Parameter: $I$ . . . . .	20
2.3.3 The Gini Parameter: $G$ . . . . .	22
2.3.4 The Multiplicity Parameter: $\Psi$ . . . . .	24
2.3.5 The Color Dispersion: $\xi$ . . . . .	26
2.3.6 Robustness of the Parameters . . . . .	27
2.4 OVERVIEW OF REST-UV SPECTRA . . . . .	35
2.4.1 Spectral Processing . . . . .	35
2.4.2 Key Spectral Features. . . . .	35
2.4.3 Equivalent Widths and Uncertainties . . . . .	38
2.5 THE RELATION OF REST-UV MORPHOLOGIES TO SPECTRA . . . . .	39
2.5.1 Interstellar Absorption Lines . . . . .	39

2.5.2	Ly $\alpha$ Emission . . . . .	43
2.5.3	Kinematic Offsets . . . . .	46
2.5.4	Rest-Optical Spectroscopic Features . . . . .	47
2.6	THE ASSOCIATION OF REST-UV MORPHOLOGIES WITH PHOTO-METRICALLY DERIVED PROPERTIES . . . . .	48
2.7	A COMPARISON OF MORPHOLOGIES WITH OTHER GALAXY SAMPLES . . . . .	54
2.7.1	AGN/QSO . . . . .	54
2.7.2	IR-Selected <i>BzK</i> Galaxies . . . . .	56
2.7.3	IR-Selected Distant Red Galaxies . . . . .	58
2.7.4	Submillimeter Galaxies . . . . .	59
2.8	DISCUSSION . . . . .	60
<b>3</b>	<b>Predictions and Strategies for Integral-Field Spectroscopy of High-Redshift Galaxies</b>	<b>66</b>
3.1	INTRODUCTION . . . . .	67
3.2	METHOD . . . . .	68
3.2.1	Signal Estimation . . . . .	69
3.2.2	Spectral Synthesis . . . . .	73
3.3	SIMULATED OBSERVATIONS WITH OSIRIS . . . . .	74
3.3.1	The OSIRIS Spectrograph . . . . .	74
3.3.2	Observing Star-Forming Regions at Intermediate-to-High Redshifts . . . . .	80
3.3.3	Signal-to-Noise Ratio Maps . . . . .	83
3.3.4	Recovery of Velocity Structure . . . . .	86
3.3.5	H $\alpha$ Morphologies and Photometry . . . . .	90
3.4	PHYSICAL LIMITATIONS . . . . .	90
3.4.1	Limiting Line Fluxes: Sampling Scales . . . . .	91
3.4.2	Limiting Line Fluxes: Telescope Aperture . . . . .	91
3.4.3	Limiting Line Fluxes: Cryogenic Considerations . . . . .	94
3.4.4	Spectral Resolution Requirements . . . . .	98
3.4.5	Benefits of Adaptive Optics . . . . .	98
3.5	SUMMARY . . . . .	99

<b>4</b>	<b>Integral Field Spectroscopy of High-Redshift Star-Forming Galaxies with Laser-Guided Adaptive Optics: Evidence for Dispersion-Dominated Kinematics</b>	<b>105</b>
4.1	INTRODUCTION . . . . .	106
4.2	OBSERVING AND DATA REDUCTION . . . . .	108
4.2.1	Sample Selection and Observational Strategy . . . . .	108
4.2.2	Reducing IFU Data . . . . .	110
4.3	NEBULAR MORPHOLOGIES . . . . .	112
4.4	GLOBAL SPECTRA . . . . .	115
4.4.1	Flux Calibration . . . . .	115
4.4.2	Global Chemistry . . . . .	118
4.4.3	Outflow Properties: UV Spectroscopy . . . . .	119
4.5	STELLAR POPULATIONS, STAR FORMATION RATES AND GAS MASSES	124
4.5.1	Stellar Masses and Stellar Populations from SED Modeling . . . . .	124
4.5.2	Star Formation Rates . . . . .	124
4.5.3	Gas Masses and Gas Fractions . . . . .	128
4.6	SPATIALLY RESOLVED KINEMATICS AND DYNAMICAL MASSES . .	130
4.6.1	Q1623-BX453 . . . . .	132
4.6.2	Q0449-BX93 . . . . .	134
4.6.3	DSF2237a-C2 . . . . .	136
4.7	DISCUSSION . . . . .	141
<b>5</b>	<b>The Kiloparsec-Scale Kinematics of High-Redshift Star-Forming Galaxies</b>	<b>150</b>
5.1	INTRODUCTION . . . . .	151
5.2	OBSERVATIONS . . . . .	153
5.2.1	Target Selection . . . . .	153
5.2.2	Observational Technique . . . . .	155
5.2.3	Data Reduction . . . . .	156
5.3	IONIZED GAS MORPHOLOGIES . . . . .	157
5.4	GLOBAL SPECTRA . . . . .	158
5.5	STELLAR POPULATION MODELING . . . . .	159
5.6	REST-UV CONTINUUM MORPHOLOGIES . . . . .	159

5.7	KINEMATIC DATA . . . . .	167
5.7.1	Q0449-BX93 . . . . .	170
5.7.2	Q1217-BX95 . . . . .	170
5.7.3	HDF-BX1564 . . . . .	174
5.7.4	Q1623-BX453 . . . . .	175
5.7.5	Q1623-BX502 . . . . .	176
5.7.6	Q1623-BX543 . . . . .	176
5.7.7	Q1700-BX490 . . . . .	178
5.7.8	Q1700-BX710 . . . . .	178
5.7.9	Q1700-BX763 . . . . .	178
5.7.10	DSF2237a-C2 . . . . .	179
5.7.11	Q2343-BX418 . . . . .	179
5.7.12	Q2343-BX513 . . . . .	179
5.7.13	Q2343-BX587 . . . . .	180
5.8	KINEMATIC MODELING . . . . .	180
5.9	DISCUSSION . . . . .	182
5.9.1	Selection Effects and the Global Population . . . . .	182
5.9.2	Relation to Complementary Surveys . . . . .	183
5.9.3	Physical Mechanisms . . . . .	188
5.A.1	QUANTIFYING THE MEAN PROPERTIES OF INCLINED SYSTEMS . . . . .	188
<b>6</b>	<b>Kpc-Scale Structure in the Nebular Emission of <math>z \sim 2.6</math> QSO Q2343-</b>	
	<b>BX415</b> . . . . .	<b>195</b>
6.1	INTRODUCTION . . . . .	196
6.2	OBSERVING AND DATA REDUCTION . . . . .	197
6.2.1	Observational Strategy . . . . .	197
6.2.2	Data Reduction and Flux Calibration . . . . .	198
6.3	GLOBAL PROPERTIES OF Q2343-BX415 . . . . .	199
6.3.1	Photometric Properties . . . . .	199
6.3.2	Spectral Properties . . . . .	200
6.4	SPATIALLY RESOLVED STRUCTURE . . . . .	205
6.4.1	Subtracting the LGSAO PSF . . . . .	205



6.4.2	Extended Emission Regions . . . . .	208
6.4.3	Detection Limits . . . . .	210
6.5	DISCUSSION . . . . .	210
6.5.1	SE Feature . . . . .	210
6.5.2	NW Feature . . . . .	212
6.6	CONCLUSIONS . . . . .	215
<b>7</b>	<b>Epilogue</b>	<b>219</b>
7.1	TOWARDS A PHYSICAL MODEL OF GALAXY FORMATION . . . . .	219
7.2	CONCLUDING REMARKS . . . . .	222
	<b>Bibliography</b>	<b>224</b>

## List of Figures

2.1	Distribution of spectroscopic redshifts . . . . .	10
2.2	<i>HST</i> -ACS rest-UV morphologies of the $z \sim 2 - 3$ galaxy sample . . . . .	12
2.2	(continued) . . . . .	13
2.2	(continued) . . . . .	14
2.2	(continued) . . . . .	15
2.2	(continued) . . . . .	16
2.3	Segmentation map of HDF-BX1035 . . . . .	19
2.4	Distribution of the morphological parameters . . . . .	21
2.5	Distribution of $G$ versus $\Psi$ . . . . .	25
2.6	<i>HST</i> -ACS images of HDF-BX1157 and HDF-BM1139 . . . . .	28
2.7	Distribution of $G$ versus $\xi$ . . . . .	29
2.8	Robustness of the morphological parameters to redshift . . . . .	31
2.9	Robustness of the morphological parameters to surface brightness . . . . .	32
2.10	<i>HST</i> -ACS rest-UV morphologies classified according to $G$ and $\Psi$ . . . . .	34
2.11	Composite rest-UV spectra . . . . .	37
2.12	Correlations between morphological and spectroscopic properties . . . . .	40
2.13	Low-ionization absorption line strengths in the $I - G$ plane . . . . .	42
2.14	Composite rest-UV spectra for a range of $G$ . . . . .	44
2.15	$\text{Ly}\alpha$ emission line strengths in the $G - M_*$ plane . . . . .	45
2.16	Composite $\text{H}\alpha$ spectra . . . . .	49
2.17	$\text{H}\alpha$ fluxes for composite stacks in the morphological parameters . . . . .	50
2.18	Histogram of UV nucleation for X-ray detected/undetected galaxies . . . . .	55
2.19	<i>HST</i> -ACS rest-UV morphologies of IR-selected <i>BzK</i> sources . . . . .	56
2.20	Comparative morphologies for $U_nGR$ , <i>BzK</i> , DRG, and SMG galaxy samples . . . . .	57

2.21	<i>HST</i> -ACS rest-UV morphologies of DRGs . . . . .	58
2.22	<i>HST</i> -ACS rest-UV morphologies of SMGs . . . . .	60
3.1	Mauna Kea background sky spectrum . . . . .	77
3.2	Time required to overcome detector read noise . . . . .	78
3.3	Relative S/N ratios achievable via binning . . . . .	79
3.4	S/N ratios as a function of redshift . . . . .	81
3.5	S/N ratio maps for four sample galaxies . . . . .	84
3.6	S/N ratio maps for different lenslet scales . . . . .	85
3.7	Velocity curve of HDF-BX1332 . . . . .	87
3.8	Model recovered velocity maps . . . . .	89
3.9	Limiting line flux density for varying lenslet scales . . . . .	92
3.10	Limiting line flux density for varying telescope diameter . . . . .	93
3.11	S/N ratios as a function of redshift for a 30 m telescope . . . . .	95
3.12	Model <i>K</i> -band background spectra . . . . .	96
3.13	Limiting line flux density for varying thermal emissivity . . . . .	97
4.1	OSIRIS maps of emission line flux and kinematics . . . . .	113
4.2	OSIRIS spectra of the target galaxies . . . . .	117
4.3	OSIRIS spectra of subregions within Q1623-BX453 . . . . .	120
4.4	Flux-calibrated UV spectra . . . . .	122
4.5	SED models for Q1623-BX453 and DSF2237a-C2 . . . . .	125
4.6	Close-up of H $\alpha$ emission from Q0449-BX93 . . . . .	134
4.7	H $\alpha$ kinematics for the faint component of Q0449-BX93 . . . . .	135
4.8	One-dimensional spectrum of DSF2237a-C2 . . . . .	137
4.9	Seeing-convolved velocity map of DSF2237a-C2 . . . . .	138
4.10	Idealized disk model for DSF2237a-C2 . . . . .	140
5.1	Spatially collapsed OSIRIS spectra . . . . .	160
5.1	(continued) . . . . .	161
5.1	(continued) . . . . .	162
5.1	(continued) . . . . .	163
5.1	(continued) . . . . .	164

5.2	SED models for the target galaxies . . . . .	165
5.2	(continued) . . . . .	166
5.2	(continued) . . . . .	167
5.3	Comparison between <i>HST</i> -ACS and OSIRIS H $\alpha$ morphologies . . . . .	168
5.4	OSIRIS maps of nebular line emission . . . . .	171
5.4	(continued) . . . . .	172
5.4	(continued) . . . . .	173
5.4	(continued) . . . . .	174
5.5	Two-dimensional NIRSPEC spectrum of HDF-BX1564 . . . . .	176
5.6	Velocity map of sub-regions with Q1623-BX543 . . . . .	177
5.7	Stellar mass versus star formation rate for the OSIRIS sample . . . . .	184
5.8	Relation between velocity shear and stellar mass . . . . .	185
6.1	Emission-line spectrum of Q2343-BX415 . . . . .	201
6.2	Comparison to long-slit NIRSPEC spectrum . . . . .	203
6.3	Previous OSIRIS spectra of Q2343-BX415 . . . . .	204
6.4	OSIRIS map of [O III] $\lambda$ 5007 Å nebular emission from Q2343-BX415 . . .	206
6.5	Radial profiles for the LGSAO PSF . . . . .	207
6.6	Spectra of residual emission features surrounding the central QSO . . . . .	209

## List of Tables

2.1	Quintile Bins for Morphological Parameters . . . . .	63
2.2	Standard Deviations from the Null Hypothesis for Independence between Morphological and Photometric Parameters . . . . .	64
2.3	Standard Deviations from the Null Hypothesis for Independence of Mor- phological Parameters and Star Formation . . . . .	65
3.1	Current Optical/IR Integral-Field Spectrographs . . . . .	101
3.2	Keck/OSIRIS System Characteristics . . . . .	102
3.3	OSIRIS Broadband Filters and Effective Model Sky Surface Brightness . .	103
3.4	Available OSIRIS Angular Lenslet Scales and Fields of View . . . . .	103
3.5	Parameters of Selected Galaxies . . . . .	104
4.1	General Information . . . . .	145
4.2	OSIRIS Morphologies . . . . .	145
4.3	Primary Spectroscopic Characteristics . . . . .	146
4.4	Secondary Spectroscopic Characteristics . . . . .	147
4.5	Q1623-BX453 Regional Emission Line Characteristics . . . . .	147
4.6	Photometric Data and SED Model Parameters . . . . .	148
4.7	Star Formation Rates and Gas Masses . . . . .	149
5.1	General Target Information . . . . .	190
5.2	OSIRIS Morphologies . . . . .	191
5.3	Nebular Line Fluxes . . . . .	192
5.4	Stellar Population Parameters . . . . .	193
5.5	Kinematic Properties . . . . .	194

6.1	General Information . . . . .	217
6.2	Q2343-BX415 Photometry . . . . .	217
6.3	Emission Lines . . . . .	218

# Chapter 1

## Introduction

Galaxies are the discrete luminous building blocks of the visible universe, tracing the development of gravitational structures across cosmic ages. The earliest galaxies at redshift  $z \sim 10$  (see, e.g., Stark et al. 2007) may have been simply glorified star-forming regions, composed of gas near the density peaks of the primordial power spectrum (e.g., Bardeen et al. 1986) which were able to decouple from the cosmic expansion at early times and form a burst of stars. As time progressed, however, these chaotic proto-galaxies gradually evolved, merging with their neighbors in newly collapsing dark halos, accreting greater quantities of gaseous fuel from a filamentary intergalactic medium, and polluting their environments with the metallic detritus of their early stellar generations. It is not until comparatively recent times ( $z \sim 1$ ) however that these early galaxies began to develop the orderly, regular morphological structures with which we are familiar in the local universe. Indeed, it is at intermediate redshifts  $z \sim 2 - 3$  (when the universe was roughly 16 – 25% of its present age) at which these morphologically irregular, juvenile galaxies are thought to have formed the majority of the stellar mass which we observe in modern-day galaxies (Dickinson et al. 2003, Reddy et al. 2008). Through a combination of galaxy-galaxy mergers, rapid star formation, and secular evolution, these galaxies experienced a strong morphological transformation into the coherent structures of the Hubble sequence which have predominated since redshift  $z \sim 1$  (Giavalisco et al. 1996; Papovich et al. 2005).

Recent years have witnessed a veritable explosion of methods for locating such galaxies. These methods include optical ( $U_nGR$ ) color selection (e.g., Steidel et al. 2003, 2004), near-IR  $BzK$  (Daddi et al. 2004) and  $J - K$  (Franx et al. 2003) color selection, and selection by sub-mm flux density (Smail et al. 1997). Of these samples, that arising from the optical

color selection is perhaps the most well studied. As described in detail by Adelberger et al. (2004), the  $U_nGR$  selection technique represents a generalized version of the Lyman-break technique employed by Steidel et al. (2003) to identify rapidly star-forming galaxies at redshift  $z \sim 3$  on the basis of their strong 912 Å Lyman break as it is redshifted into the  $U_n$  bandpass. In this thesis, we focus primarily on this  $U_nGR$  sample, and particularly on those galaxies in the redshift ranges  $z = 1.8 - 2.6$  (i.e., the “BX” galaxy sample of Steidel et al. 2004) and  $z = 2.6 - 3.4$  (i.e., the “LBG” sample of Steidel et al. 2003). As detailed by Adelberger et al. (2004), these redshift ranges are dictated by the selection functions of the respective color selection criteria. While initial identification of these galaxies was based upon photometric preselection, extensive spectroscopic follow-up work has derived precise redshifts for all galaxies in our primary target sample.

The galaxies selected in this manner are typically bright and actively forming stars, with extinction-corrected star formation rates (SFR)  $\gtrsim 30 M_\odot \text{ yr}^{-1}$  (see discussion by Erb et al. 2006b), and SFR surface densities similar to those observed in local starburst galaxies (e.g., Kennicutt et al. 1998b). The resulting winds from supernovae and massive stars drive energetic ( $\sim 500 \text{ km s}^{-1}$ ; Steidel et al. *in prep.*) large-scale outflows into the IGM surrounding these galaxies, creating the ubiquitous blueshifted interstellar absorption features observed in rest-frame UV spectra (e.g., Shapley et al. 2003). With the aid of deep near-IR (e.g., Erb et al. 2006c) and mid-IR (e.g., Papovich et al. 2006; Reddy et al. 2006b; and references therein) photometry, stellar population modelling suggests that galaxies at  $z \sim 2 - 3$  span a broad range of stellar masses and evolutionary states.

Despite our growing knowledge of the broad global characteristics of  $z \sim 2 - 3$  galaxies, however, our knowledge of their internal structure and dynamical evolution has been limited by their small angular size (typically  $\lesssim 1$  arcsecond). Such objects are generally not well resolved in the ground-based imaging and spectroscopy which form the backbone of the observational data, precluding us from determining (for instance) the triggering and regulation mechanisms of these starbursts, whether this star formation occurs in nuclear or circum-nuclear regions of dynamically relaxed systems or as a result of tidal shocks induced by major mergers, and whether individual regions of star formation follow a global abundance pattern or exhibit strong variations in chemical enrichment. Each of these distinctions has appreciable implications for the evolution and development of structure and



stellar populations within a given galaxy. In this thesis, we capitalize on recent technological developments to explore what information can be gleaned from such spatially resolved information. We describe our specific goals in greater detail below.

## 1.1 MORPHOLOGY

One method of probing the small-scale structure and distribution of star formation is through deep wide-field imaging with space-based optical telescopes such as *HST* which are not subject to the atmospheric turbulence which limits ground-based facilities. In particular, the optical-wavelength Advanced Camera for Surveys (ACS) and the near-IR camera NICMOS provide high-quality imaging with spatial resolutions of 0.5 kpc and 1.6 kpc, respectively, at redshift  $z \sim 2$ . Such studies are particularly appealing given the wealth of information contained in the distribution of luminous matter (i.e., the morphology) within local Hubble-type galaxies, from which it is typically possible to deduce kinematics, rate and distribution of star formation, and the recent merger history. Unsurprisingly, numerous studies (e.g., Abraham et al. 2003; Conselice et al. 2003, 2006; Chapman et al. 2003; Lotz et al. 2004, 2006) have therefore sought to characterize the morphologies of  $z \sim 2 - 3$  galaxies in order to derive information about their internal structure and interaction histories.

At redshifts  $z \sim 2 - 3$  however, the majority of the galaxy population have highly irregular morphologies, frequently composed of multiple spatially separated components, which bear little similarity to the local Hubble-type population (Giavalisco et al. 1996; Papovich et al. 2005). This has commonly been assumed to indicate the wide-spread prevalence of major galaxy–galaxy mergers at this cosmic epoch, but it is uncertain whether these structures are predominantly caused by merger activity, patchy star formation, dust extinction, or some other physical process (and likely a combination of all of the above). Consequently, it is far from certain whether morphological information alone can reveal anything about the star formation history, mass, or kinematics of these galaxies. As a first step in understanding the resolved structure of the high-redshift galaxy sample, a comprehensive study of the physical interpretation of galaxy morphology at high redshift (i.e., how morphology relates to the derived stellar mass, star formation rate, outflow properties, etc.) is therefore warranted to ascertain whether morphological information alone can provide a meaningful characterization of the small-scale structure and mass assembly history of galaxies.

## 1.2 KINEMATICS

An approach which is both more time consuming and perhaps more promising is studying the ionized gaseous structure surrounding bright star-forming regions produced by the flood of energetic photons from these young stars. Excited atoms in this gas lose energy predominantly by emission of strong rest-frame optical nebular emission lines (redshifted into the near-IR for galaxies at  $z \sim 2 - 3$ ) such as  $H\alpha$ ,  $[O\ III]$ , and  $[N\ II]$ . The relative strengths of these lines encodes information about the chemical composition of the gas and the shape of the ionizing spectrum, permitting deduction of the metallicity and star formation rates of the emission regions. These emission features are also intrinsically narrow, and the central wavelength and widths of the lines can therefore be used to derive precise relative velocities and kinematic dispersions among star-forming regions along a given line of sight.

Such information is critical for answering a number of outstanding questions, not least of which is the mechanism by which galaxy formation and gas accretion occurs in the young universe. According to basic theories of galaxy formation (e.g., White & Rees 1978) hot-mode accretion dominates the gas accretion history of galaxies. Once a sufficiently massive dark matter halo has virialized, gas can fall into its potential well, heating via shocks to the virial temperature of the host halo. As this gas cools over time it collapses to form a rotating disk supported by angular momentum which the cooled gas has been unable to shed. This gaseous disk is posited to be the home of the bulk of active star formation. The actual mechanism of dynamical support for galaxies at  $z \sim 2 - 3$  is unknown, however, posing a crucial test for this theory.

Studies using slit (e.g., Erb et al. 2004, 2006b, 2006c; Weiner et al. 2006) spectroscopy have met with qualified success and demonstrated that the kinematics of these galaxies are frequently inconsistent with the gas-disk models (although c.f. Förster-Schreiber et al. 2006), often exhibiting kinematics that appear to be dominated by velocity dispersion rather than identifiable shear. However, these studies have been limited by the small angular size of typical galaxies relative to the atmospheric seeing. Not only may there typically be only 1–2 spatially uncorrelated samples across the face of a given galaxy, but additional uncertainty may be introduced by misalignment of the slit with the kinematic axis. It is therefore unclear whether the observed dispersion is *intrinsic* to the target galaxies, or caused by the smearing out of unresolved kinematic structure.

The recent advent of adaptive optics (AO) on 10 m class telescopes offers for the first time the opportunity to overcome the limitations previously imposed by atmospheric turbulence by rapidly correcting the distorted wavefront using deformable mirrors. While originally proposed over 50 years ago (Babcock et al. 1953), it is only in the last 10–15 years that advances in computer technology have made such an idea possible, albeit restricted to targets located near bright reference stars used to determine the wavefront corrections. The development of artificial laser-generated guide stars (LGSAO; see, e.g., discussion by Wizinowich et al. 2006) has greatly expanded the available sky coverage of this technique, permitting observation of the majority of deep-sky targets. Paired with integral-field spectroscopy, it is possible to obtain diagnostic spectra of spatial regions resolved on scales of order 100 milliarcseconds (corresponding to roughly 1 kpc at redshift  $z \sim 2 - 3$ ). The data provide an empirical answer to whether the velocity fields of galaxies in the early universe are predominantly represented by virialized disk-like systems, major mergers, or some other dynamical structure, and whether the resulting star formation is uniform in its properties across a given galaxy or exhibits regional variation on scales of a kiloparsec.

The outline of this thesis is as follows: In Chapter 2 (Law et al. 2007b) we describe our morphological analysis of redshift  $z \sim 2 - 3$  galaxies in the GOODS-N field. Using a variety of methods to characterize their irregular morphologies, we discuss the physical interpretation of galaxy morphology in light of photometric and spectroscopic measures of the galaxies' component stellar populations. We then proceed to explore the spatially resolved kinematics of these galaxies using the new OSIRIS (OH-Suppressing InfraRed Imaging Spectrograph; Larkin et al. 2006) integral field spectrograph in conjunction with the Keck Observatory LGSAO system. In Chapter 3 (Law et al. 2006) we discuss the capabilities and limitations of this spectrograph prior to our observing program. Results for 3 galaxies obtained early in this program are presented in Chapter 4 (Law et al. 2007a). These early results are extended using observations of an additional 10 galaxies discussed in Chapter 5. In a separate article (included here as Chapter 6) we demonstrate the capability of these LGSAO data to determine the properties of galaxies which host luminous QSOs in addition to ordinary star-forming galaxies. Finally, in Chapter 7 we summarize our conclusions regarding the physical structure and formation history of  $z \sim 2 - 3$  galaxies and describe the implications of these data for theoretical models of galaxy formation.

## Chapter 2

# The Physical Nature of Rest-UV Galaxy Morphology During the Peak Epoch of Galaxy Formation<sup>\*</sup>

DAVID R. LAW<sup>a</sup>, CHARLES C. STEIDEL<sup>a</sup>, DAWN K. ERB<sup>b</sup>, MAX PETTINI<sup>c</sup>,  
NAVEEN A. REDDY<sup>a</sup>, ALICE E. SHAPLEY<sup>d</sup>, KURT L. ADELBERGER<sup>e</sup>, DAVID J. SIMENC<sup>a</sup>

<sup>a</sup>California Institute of Technology, MS 105–24, Pasadena, CA 91125

<sup>b</sup>Harvard-Smithsonian Center for Astrophysics, MS 20, 60 Garden St, Cambridge, MA 02138

<sup>c</sup>Institute of Astronomy, Madingley Road, Cambridge CB3 0HA, UK

<sup>d</sup>Department of Astrophysical Sciences, Princeton University, Peyton Hall, Ivy Lane, Princeton, NJ 08544

<sup>e</sup>McKinsey and Company, 1420 Fifth Avenue, Suite 3100, Seattle, WA 98101

## Abstract

Motivated by the irregular and little-understood morphologies of  $z \sim 2 - 3$  galaxies, we use non-parametric coefficients to quantify the morphologies of 216 galaxies which have been spectroscopically confirmed to lie at redshifts  $z = 1.8-3.4$  in the GOODS-N field. Using measurements of ultraviolet (UV) and optical spectral lines, multi-band photometric

---

<sup>\*</sup>A version of this chapter was published in *The Astrophysical Journal*, 2007, vol. 656, 1–26, and is reproduced by permission of the AAS.

data, and stellar population models we statistically assess possible correlations between galaxy morphology and physical observables such as stellar mass, star formation rate, and the strength of galaxy-scale outflows. We find evidence that dustier galaxies have more nebulous UV morphologies and that larger, more luminous galaxies may drive stronger outflows, but otherwise conclude that UV morphology is either statistically decoupled from the majority of physical observables or determined by too complex a combination of physical processes to provide characterizations with predictive power. Given the absence of strong correlations between UV morphology and physical parameters such as star formation rates, we are therefore unable to support the hypothesis that morphologically irregular galaxies predominantly represent major galaxy mergers. Comparing galaxy samples, we find that IR-selected  $BzK$  galaxies and radio-selected submillimeter galaxies (SMGs) have UV morphologies similar to the optically selected sample, while distant red galaxies (DRGs) are more nebulous.

## 2.1 INTRODUCTION

In the local universe the projected distribution of luminous matter within a galaxy, i.e., the morphology, often provides a wealth of information about that galaxy’s kinematics, rate of star formation, and recent merger history. In the classical picture, late-type spiral galaxies harbor active star formation in the gas-rich arms of a flattened rotating disk, while early-type elliptical galaxies tend to be more massive, dispersion-supported, and quiescent systems. At high redshifts from  $z \sim 2 - 3$ , however, the morphologies of typical galaxies are highly irregular (Abraham et al. 1996; Kajisawa & Yamada 2001; Conselice et al. 2005), frequently composed of multiple spatially separated components, and appear to bear little similarity to the local Hubble-type population. It is uncertain whether these irregular morphologies are due to patchy star formation, prevalent merger activity, or some other physical process, and consequently unknown whether these morphologies can (analogously to local galaxies) tell us anything about the star formation rate, mass, or stellar kinematics of galaxies at high redshifts.

Since morphological studies are often performed at optical wavelengths which probe rest-frame ultraviolet (UV) radiation for galaxies at redshifts  $z \gtrsim 1$ , one might *expect* that the morphologies of such galaxies should appear irregular, since radiation at such wavelengths

predominantly traces emission from the brightest active star-forming regions rather than the redder bulk of the stellar population (Dickinson 2000). UV emission tends to be patchy and irregular even for local Hubble-type galaxies (e.g., Gordon et al. 2004), as in the case of the local galaxy merger VV 114 (whose broad rest-UV absorption line spectra suggest that it may be a local analog to  $z \sim 2 - 3$  Lyman Break Galaxies; Grimes et al. 2006) whose near-infrared (NIR) morphology clearly shows a pair of interacting late-type galaxies while the rest-UV morphology shows only scattered clumps of emission (Goldader et al. 2002). However, high-redshift galaxies have irregular morphologies not only in the rest-UV, but often at rest-optical wavelengths as well (Dickinson 2000; Papovich et al. 2005), indicating that (in contrast to local galaxies) both wavelength regimes are dominated by emission from young starbursting components and therefore that there may be some fundamental difference between the two samples.

One popular explanation for these multi-component, irregular morphologies is that they represent major merger systems, and that their prevalence indicates that the rate of major mergers was much greater at high redshifts than in the local universe (e.g., Conselice et al. 2003). Such a conclusion fits well within the framework of cold dark matter (CDM) theory, and may additionally be supported by stellar population analyses (e.g., Dickinson et al. 2003) which suggest that many galaxies in the local universe accumulated a large fraction of their stellar mass at  $z \sim 2 - 3$ , as might be expected if star formation peaked in this epoch as a result of tidally induced collapse spurred by major mergers. However, the interpretation of a multi-component or otherwise irregular morphology is not always clear. In the case of VV 114, near-IR imaging (Goldader et al. 2002) indicates that all of the clumps of UV emission are associated with only one galaxy of the merger pair and that the multi-component UV morphology therefore directly reflects clumpy star formation rather than tracing tidally distorted features from each of the two galaxies.

Building on a body of literature characterizing the morphologies of galaxies at redshifts  $z \sim 2 - 3$  (e.g., Abraham et al. 2003; Conselice et al. 2003; Lotz et al. 2004, 2006; Ravindranath et al. 2006) it is worthwhile to ask whether rest-UV morphologies correspond to any other physical observables such as UV/optical spectral line strengths (e.g., Shapley et al. 2003; Erb et al. 2006a), stellar population models (e.g., Shapley et al. 2005b; Erb et al. 2006a; Reddy et al. 2006a), or rest-optical to IR properties (e.g., Reddy et al. 2006a,

2006b). In this work, we use non-parametric coefficients to characterize the morphologies of 216 spectroscopically confirmed galaxies in the redshift range  $z = 1.8 - 3.4$ , assess the statistical significance of correlations with spectrophotometric observables, and discuss the resulting physical interpretation of galaxy morphology. In §2.2 we describe our galaxy sample and give a basic description of the sample population. In §2.3 we outline our morphological parameters, comparing our results to the recent studies of Conselice et al. (2003) and Lotz et al. (2004, 2006). Rest-frame UV spectra are introduced in §2.4, correlations between morphology and spectral line strength and kinematics are discussed in §2.5. In §2.6 and §2.7 we compare morphologies with stellar population models derived from UV to mid-IR photometric data, as well as discussing differences between different samples of high-redshift galaxies and AGN selected on the basis of various photometric criteria. Finally, we discuss the implications of our results for the physical interpretation of galaxy morphologies in §2.8. Our morphological statistics and ancillary data are made publically available in an electronic database located at <http://www.astro.caltech.edu/~drlaw/GOODS/>.

We assume a standard  $\Lambda$ CDM cosmology in which  $H_0 = 71 \text{ km s}^{-1} \text{ Mpc}^{-1}$ ,  $\Omega_m = 0.27$ , and  $\Omega_\Lambda = 0.73$ .

## 2.2 SAMPLE SELECTION

Our sample is drawn from rest-UV color-selected catalogs of  $z \sim 2 - 3$  star-forming galaxy candidates (Steidel et al. 2003, 2004; Adelberger et al. 2004) in the GOODS-N field. These catalogs are based on deep ground-based imaging, and therefore select galaxies independent of morphology or surface brightness since even the largest galaxies are nearly unresolved in these seeing-limited images. We consider only those galaxies which have been spectroscopically confirmed to lie in the redshift intervals  $z = 1.8 - 2.6$  or  $z = 2.6 - 3.4$  (i.e., the peak redshift ranges defined by the selection functions of the color selection criteria, see Adelberger et al. 2004) and which exhibit no obvious spectroscopic signatures of active galactic nuclei.

The redshift distribution of galaxies in our sample is shown in Figure 2.1: the  $z \sim 2$  sample contains 150 galaxies in the range  $1.8 < z < 2.6$  with mean  $\bar{z} = 2.17 \pm 0.21$ , while the  $z \sim 3$  sample contains 66 galaxies in the range  $2.6 < z < 3.4$  with  $\bar{z} = 3.02 \pm 0.19$ .

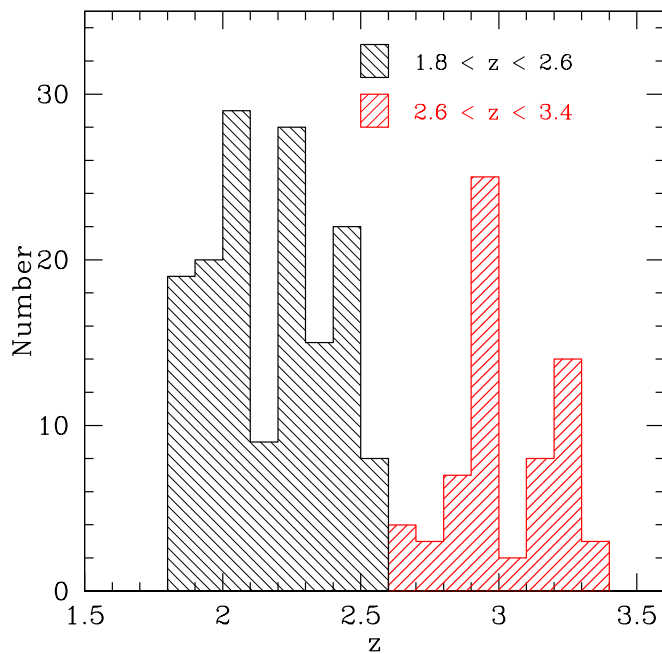


Figure 2.1 Distribution of galaxies with spectroscopic redshift  $z$ .

## 2.3 MORPHOLOGIES

Morphological parameters were determined from deep *HST*-ACS imaging obtained as part of the GOODS-N survey (Giavalisco et al. 2004) in F435W ( $B$ ), F606W ( $V$ ), F775W ( $I$ ), and F850LP ( $z$ ) bandpasses with drizzled pixel scale of  $50 \text{ mas pixel}^{-1}$  and  $10\sigma$  limiting point source sensitivities of 27.8, 27.8, 27.1, and 26.6 mag (AB) respectively (Giavalisco et al. 2004). At redshifts  $z \sim 2$  and  $z \sim 3$  these bandpasses collectively probe rest-frame UV emission in the wavelength intervals  $\sim 1500 - 3000 \text{ \AA}$  and  $\sim 1000 - 2000 \text{ \AA}$ , respectively.

The observed morphology is qualitatively similar throughout this range of wavelengths (see §2.3.6), and we therefore improve our signal-to-noise ratios per pixel by creating a single rest-frame UV image from a weighted sum of the four individual bandpasses. Weights for this sum are determined proportionally to the inverse variance of the overall sky noise relative to the average number of counts from the  $z \sim 2 - 3$  galaxies. The UV composite morphologies of our 216 galaxies are shown in Figure 2.2 in order of increasing redshift, and demonstrate a variety of morphological types ranging from single nucleated<sup>1</sup> sources

<sup>1</sup>We adopt the term “nucleation” to qualitatively describe a concentrated region of flux which might naively be described as the “nucleus” of a given galaxy. This contrasts with the term “nebulousity” which we



to extremely asymmetric sources with multiple nucleations and/or nebulous components. The “typical” galaxy has a morphology comprising one or more spatially distinct clumps with some degree of diffuse nebulosity, reminiscent of the HST-*STIS* UV morphology of the local interacting galaxy VV 114 (Goldader et al. 2002) which is dominated by a patchy distribution of star formation regions. Our initial morphological classification groups galaxies by visual inspection on the basis of the apparent nucleation of their light profiles and the presence and number of multiple nucleated emission components. Galaxies fall within five general classes:

1. Single strongly nucleated sources (11 sources at  $z \sim 2$ , 9 sources at  $z \sim 3$ ).
2. Multiple strongly nucleated sources (6 sources at  $z \sim 2$ , 2 sources at  $z \sim 3$ ).
3. Single nucleated source accompanied by nebulosity (61 sources at  $z \sim 2$ , 27 sources at  $z \sim 3$ ).
4. Multiple nucleated sources accompanied by nebulosity (35 sources at  $z \sim 2$ , 12 sources at  $z \sim 3$ ).
5. Nebulous emission with no strong nucleation (37 sources at  $z \sim 2$ , 16 sources at  $z \sim 3$ ).

We seek a set of numerical parameters which will allow us to effectively reproduce these intuitive divisions, while providing a more rigorous mathematical basis for the classification. The “*CAS*” system of parameters has recently been a popular choice, characterizing galaxies on the basis of their concentration ( $C$ ; Kent 1985, Bershady et al. 2000), asymmetry ( $A$ , Schade et al. 1995), and clumpiness ( $S$ , Conselice et al. 2003). However, the first two of these quantities are explicitly defined with regard to circular or elliptical apertures measured about a central point, which is only well defined for galaxies with morphologies similar to traditional elliptical or spiral galaxies, while the third quantity relies upon suitable choice of a smoothing scale on which clumpiness is defined. In the case of the  $z \sim 2 - 3$  galaxy sample, morphologies are generally so irregular (see Fig. 2.2) that they do not have a well-defined “center”, and the measured values of the *CAS* parameters can depend strongly 

---

use to describe diffuse flux which is spread fairly uniformly over a number of pixels.